OR/12/023 Results

From Earthwise
Jump to navigation Jump to search

Wragg, J, Rushton, J, Bateman, K, Green, K, Harrison, H, Wagner, D, Milodowski, A E, and West, J M. 2012. Microbial Impacts of CO2 transport in Sherwood Sandstone. *British Geological Survey Internal Report*, OR/12/023.

Characteristics of the sandstone starting materials

X-ray diffraction analysis

The starting material has previously been analysed and the results reported by West et al., (2011)[1]. In summary, the sample comprises of major amounts of quartz, minor amounts of feldspars (K-feldspar and plagioclase) and 'mica' (undifferentiated mica species possibly including muscovite, biotite, illite, illite/smectite etc) and trace amounts of chlorite and hematite. The clay fraction (<2 µm) is composed of illite, illite-smectite mixed-layer clay and chlorite.

Characteristics of the post-experimental materials

Whole rock mineralogical analysis results

The results of whole-rock XRD analyses of the post-experimental control samples and biotic residues that were taken at 10–20 mm intervals along the column are summarised in Tables 2 and 3.

XRD analysis showed that the samples are predominantly composed of quartz, minor amounts of feldspars (K-feldspar and plagioclase), dolomite and 'mica' (undifferentiated mica species possibly including muscovite, biotite, illite, illite/smectite etc.) and trace amounts of chlorite, halite and hematite. Trace amounts of amphibole were detected in the biotic residue at 0–10 mm from column inlet.

No significant differences between the control materials and biotic residues were detected.

Table 2 Whole-rock X-ray diffraction analysis of control samples.

Subsamples taken from column inlet in mm	**MPL Code**	**Mineralogy (%)**							
		albite	**chlorite**	**dolomite**	**halite**	**hematite**	**K-feldspar**	**'mica'**	**quartz**
0–20	MPLQ632	4.8	0.6	4.7	<0.5	<0.5	12.8	1.8	74.7
20–40	MPLQ633	5.4	0.6	5.3	<0.5	<0.5	12.3	2.4	73.4
40–60	MPLQ634	5.0	<0.5	5.5	<0.5	<0.5	12.9	1.9	73.9
>60	MPLQ635	4.4	<0.5	5.8	<0.5	<0.5	13.0	1.8	74.3

Table 3 Whole-rock X-ray diffraction analysis of biotic residues.

Subsamples taken from column inlet in mm	**MPL Code**	**Mineralogy (%)**								
		albite	**amphibole**	**chlorite**	**dolomite**	**halite**	**hematite**	**K-feldspar**	**'mica'**	**quartz**
0–10	MPLQ861	4.6	<0.5	0.8	5.5	<0.5	<0.5	13.3	2.0	73.2
10–20	MPLQ862	4.8	nd	0.7	5.2	<0.5	<0.5	13.6	1.8	73.5

30–40	MPLQ863	4.8	nd	0.7	4.5	<0.5	<0.5	13.5	2.0	74.2
40–60	MPLQ864	5.0	nd	0.5	4.5	<0.5	<0.5	13.1	2.0	74.6
>60	MPLQ865	5.2	nd	0.5	5.5	<0.5	<0.5	12.7	2	73.7

Key
nd — not detected
'mica' = undifferentiated mica species including muscovite, biotite, illite and illite/smectite etc.

Clay mineralogy

The results of XRD analysis of the <2 µm materials of the control samples and biotic residues showed that the clay mineral fraction is composed of illite, illite-smectite mixed-layer clay and chlorite.

The biotic sample residues at '0–10 mm' and '10–20 mm' from column inlet also exhibited a small peak at c. 16.7Å after ethylene glycol salvation, suggesting the presence of trace amounts of smectite (estimated <1% of the clay fraction). This was observed neither in the original core samples nor in any of the control samples and may be linked to the introduction of microbes. However, longer duration experiments are needed to make definitive conclusions, as it is possible that this is just an artefact of sample heterogeneity (e.g. laminations within the sandstone).

A labelled clay mineral XRD trace of the biotic sample taken at '0–10 mm' is shown in Appendix 1.

Non-swelling clays

The 'non-swelling clays' illite, and chlorite were identified in all the samples:

Illite was identified by its characteristic air-dry *d*001 spacing of c. 10.0Å which remains invariant after glycol-solvation and heating.

Chlorite was identified by its characteristic air-dry and glycol-solvated basal spacing peaks at 14.2, 7.1, 4.73 and 3.54Å and particularly the presence of a peak at c. 13.5Å after heating at 550°C.

Swelling clays

The illite/smectite detected in the samples is characterised by a broad *d*001/002 peak at c. 11.6Å on the air dry trace and a peak at c. 12.8Å on glycol-solvation. Heating to 550°C causes the peak to collapse to a c. 9.6Å spacing.

Petrography

Control sample

Samples were analysed from the inlet end of the post-test control plug and from 40–50 mm into the sample from the inlet face. Plates 7 to 12 are example SEM images of the post control test material.

At the inlet end, some pore walls were observed to be thinly and patchily coated by a film-like phase. This film was typically associated with deposits of silicate fines. These fines were either mobilised during testing or by post-testing sample preparation. In detail the film locally has a fibre-like content. Under the electron beam of the SEM and at ESEM chamber humidities <100%, the film was noted to shrink, suggesting it has a high water content. Rare cell-like textures were noted as <2 µm rounded forms on pore walls.

A similar film was also identified at the 40–50 mm depth within the post-test sample material, although of considerably reduced abundance. Again, the film locally has a filamentous content, is associated with silicate fines, and shrinks under the electron beam and at reduced humidities. No cell-like features were identified, however.

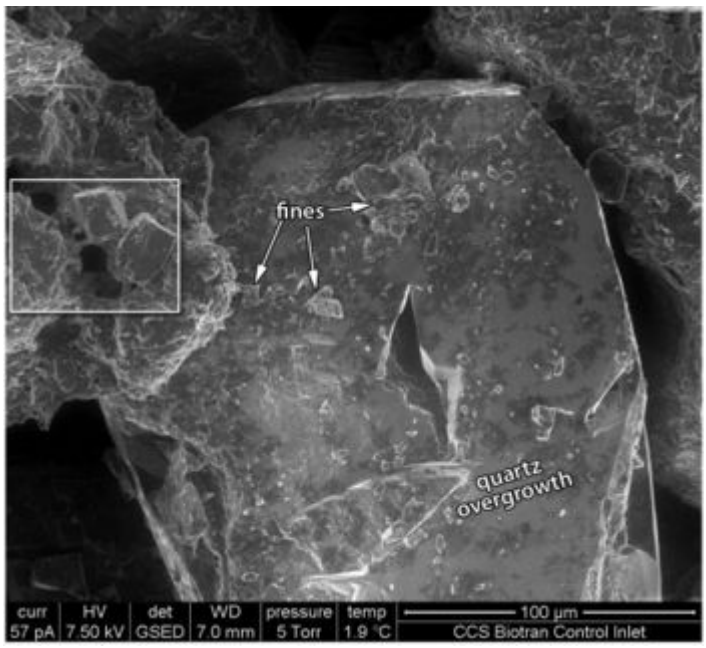

- **Plate 7** SEM image. Post test control sample, inlet end, 95% humidity. A patchy dark film-like deposit on the pore walls, much of it here defined by quartz overgrowth, is typically associated with deposits of mobilised fines. Boxed area is the site of the following plate.

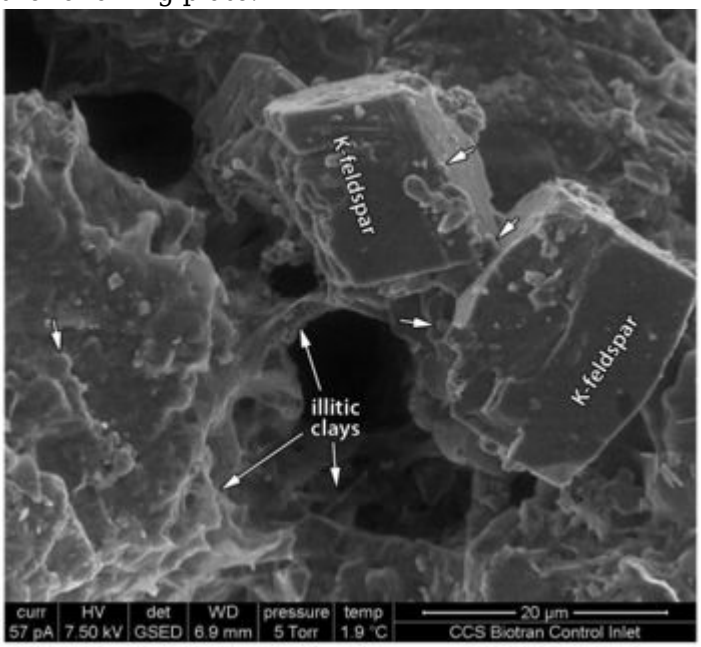

- **Plate 8** SEM image. Post test control sample, inlet end, 95% humidity. From the boxed area in the preceding image. Diagenetic features include authigenic K-feldspars and illitic clays bridging a pore throat. There are scattered oval and rounded forms about 2 µm across scattered on pore walls.

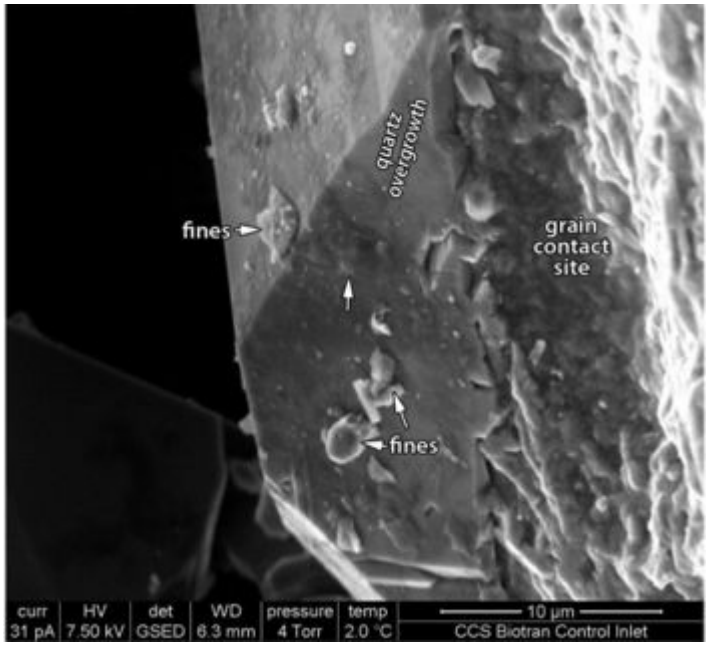

Plate 9 SEM image. Post test control sample, inlet end, 80% humidity. A quartz overgrowth is partially coated by a thin film-like phase. There are mineral fines deposited on the surface of the film.

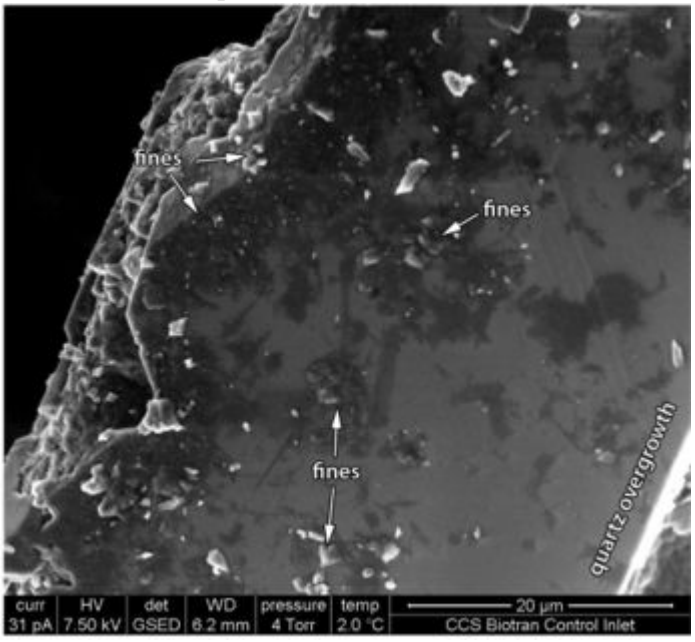

Plate 10 SEM image. Post test control sample, inlet end, 80% humidity. A quartz overgrowth is partially coated by a thin film-like phase, commonly with a filamentous form. There are widespread mineral fines deposited on the surface of the film.

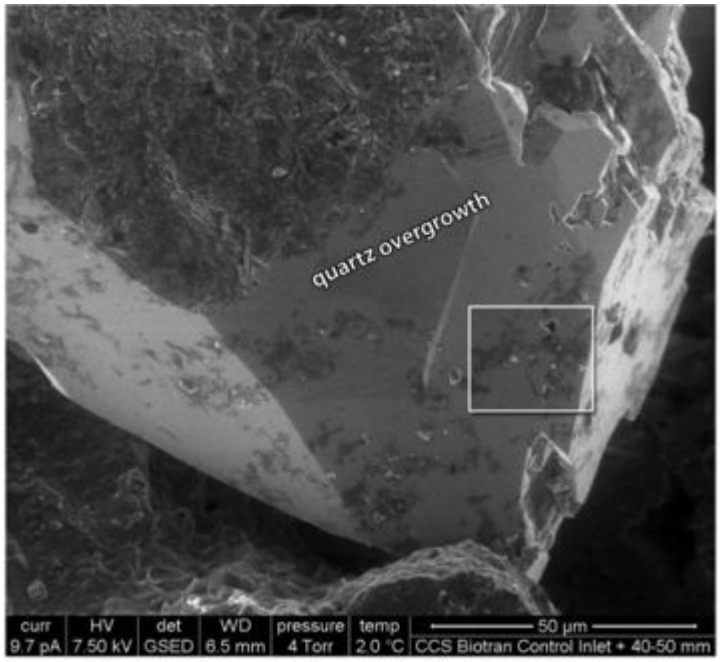

Plate 11 SEM image. Post test control sample, from 40–50 mm beyond the inlet face, 80% humidity. Pore walls, here defined by quartz overgrowth, have a sparse and patchy film-like coating. Boxed area is the site of the following plate.

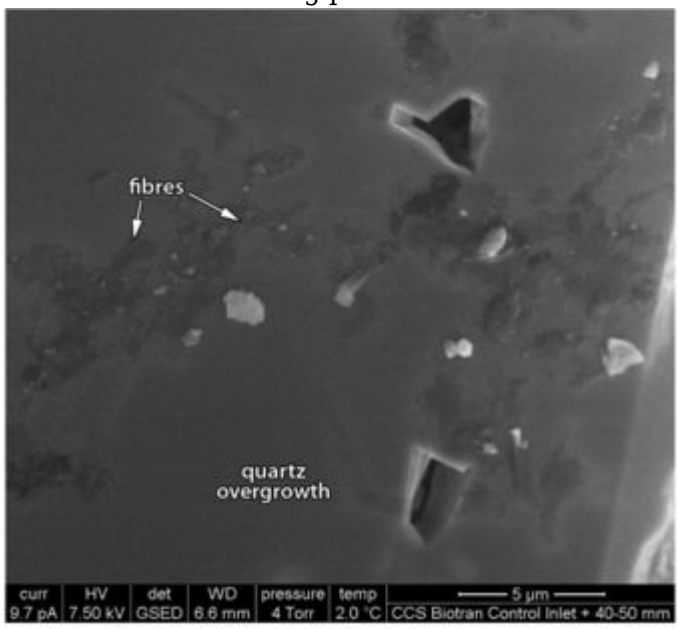

Plate 12 SEM image. Post test control sample, from 40–50 mm beyond the inlet face, 80% humidity. Detail of the patchy film-like coating from the boxed area in the preceding plate. Again, the film is typically associated with fines. In detail the film commonly has a fibrous aspect.

Biotic sample

Upon removal of the biotic sample from the test apparatus, it was noted that a portion of the test plug had a grey stain visible at its outlet end (Plate 13, Plate 14 and Plate 15). Upon splitting the plug as part of the sample preparation, it was further noted that this staining was only present at the

outside surface; it did not appear to have penetrated the sample to any significant depth (Plate 16).

Samples were taken and analysed from the inlet end of the post-test biotic plug, from 40 mm into the sample from the inlet face, and from the outlet end. At each of these sampling points, samples were prepared from the centre and from the edge of the plug. One edge sample from the outlet end was prepared to include an area affected by the grey staining to enable this to be examined.

- 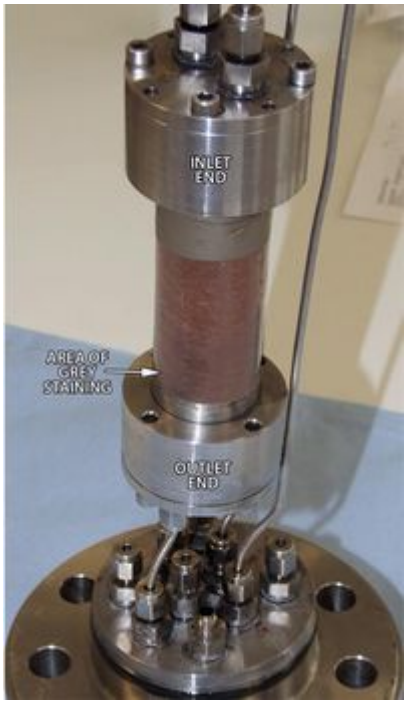

Plate 13 Biotic sample during decommissioning, showing the test plug contained in the apparatus. An area of grey staining is apparent at the outlet end of the plug.

- 

Plate 14 Test plug and end frits after removal of the outer casing, showing the patch of grey stain on the outside at the outlet end. Bedding planes are indicated.

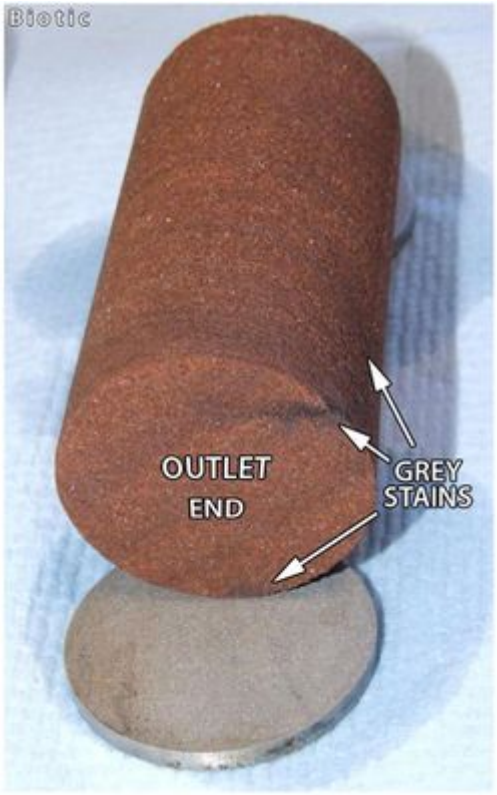

Plate 15 Outlet end of the test plug showing the extent of the grey staining.

Plate 16 Biotic test plug freshly fractured, showing the strongly defined bedding structures. The grey staining observed on the outside of the plug has not penetrated the plug interior.

Inlet end

At the inlet end most pore walls were observed to be thinly and patchily coated by a film-like phase (Plate 17 to Plate 20). This film was typically associated with collections of silicate fines that appear to be affixed by the film (Plate 19). These fines were either mobilised during testing or by post-testing sample preparation. Under the electron beam and at ESEM chamber humidity's <100%, the film was noted to shrink, suggesting it has a high water content. There are widespread cell-like textures associated with many of the patches of film, typically embedded as <3 µm oval, rounded forms (Plate 19, Plate 20).

In detail the film locally has a fibre-like content (Plate 18). These fibres are similar to a diagenetic fibrous illite locally recognisable as a grain-coating (Plate 25) and pore-bridging constituent of the host rock.

- 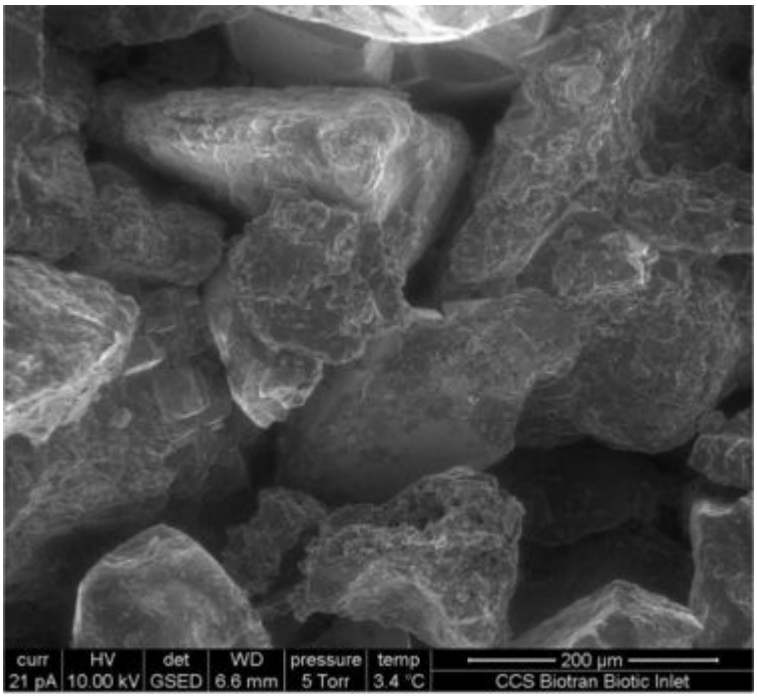

Plate 17 SEM image. Post test biotic sample, central inlet end, 90% humidity. General view showing scattered patches of a film-like deposit on pore walls, several with associated silicate fines.

- 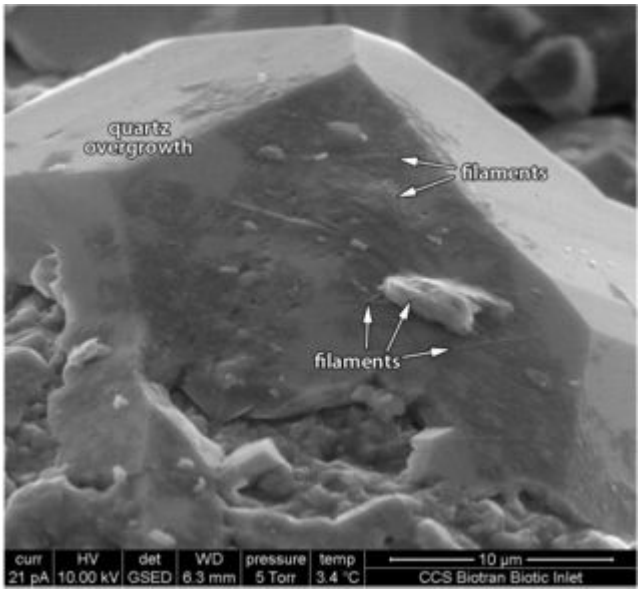

Plate 18 SEM image. Post test biotic sample, central inlet end, 90% humidity. Detail of a quartz overgrowth with a patchy film-like deposit. A filamentous phase associated with the film is also visible draped over the top of an angular fragment of silicate. This is most likely a fibre of illitic clay.

- 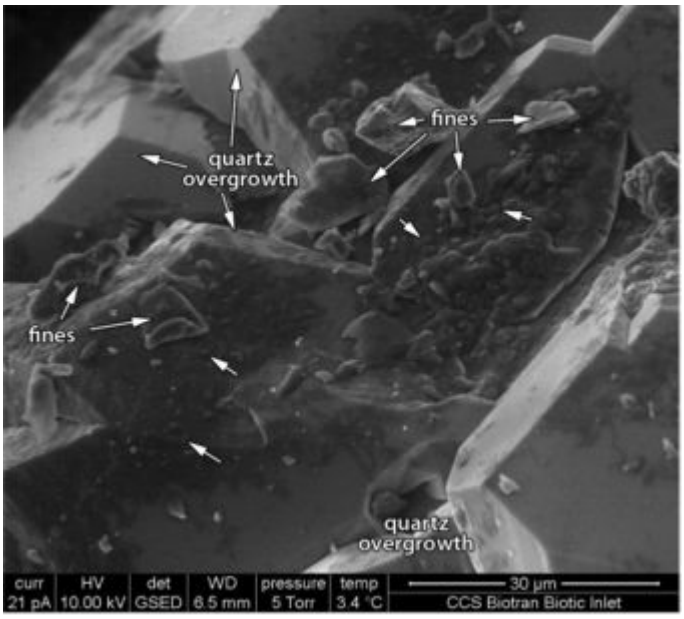

Plate 19 SEM image. Post test biotic sample, central inlet end, 90% humidity. This area of pore wall defined by quartz overgrowth is partially coated by film and associated fines. There are scattered rounded oval forms <3 µm across visible within the film (unlabelled arrows).

- 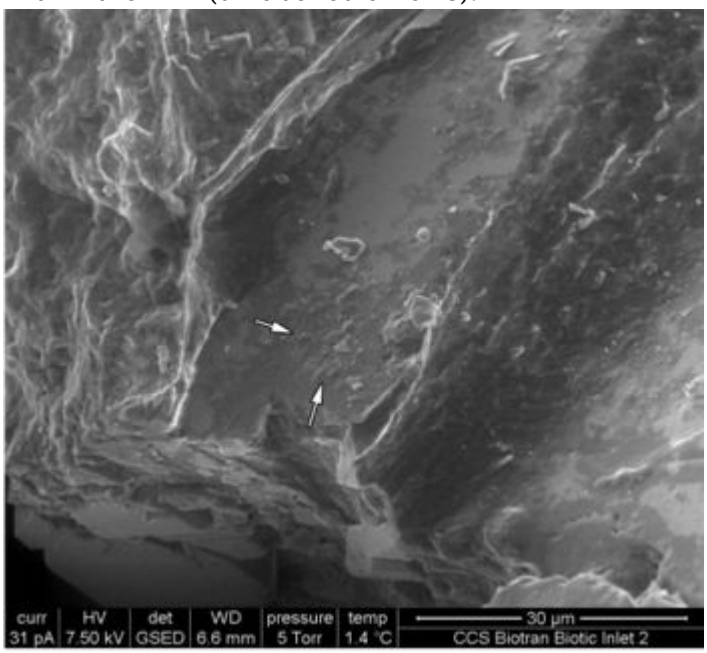

Plate 20 SEM image. Post test biotic sample, edge inlet end, 90% humidity. This area of pore wall has a patchy film coating that contains common rounded, oval <3 µm forms (unlabelled arrows).

Inlet + 40 mm

A similar film to that observed in the inlet material was identified at the 40 mm depth point within the post-test sample material (Plate 21), with a slightly reduced abundance. Again, the film is typically associated with apparently adhered silicate fines (Plate 21 and 22), and shrinks under the electron beam and at reduced humidities. Cell-like features were rarely identified (Plate 22). Film was identified both in the central and edge samples.

At some sites where pore walls extend towards the centres of pores, film and associated fines appear to be more abundant (Plate 22); these sites are likely to have been extending into more rapidly moving test fluids.

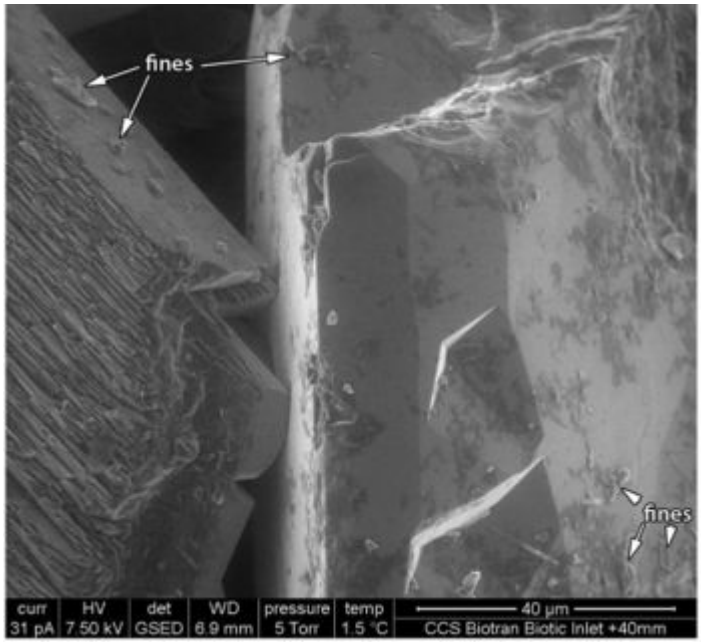

Plate 21 SEM image. Post test biotic sample, central inlet + 40 mm, 95% humidity. Typical patchy pore lining film with associated fines on quartz (centre, right) and K-feldspar (left) overgrowth faces.

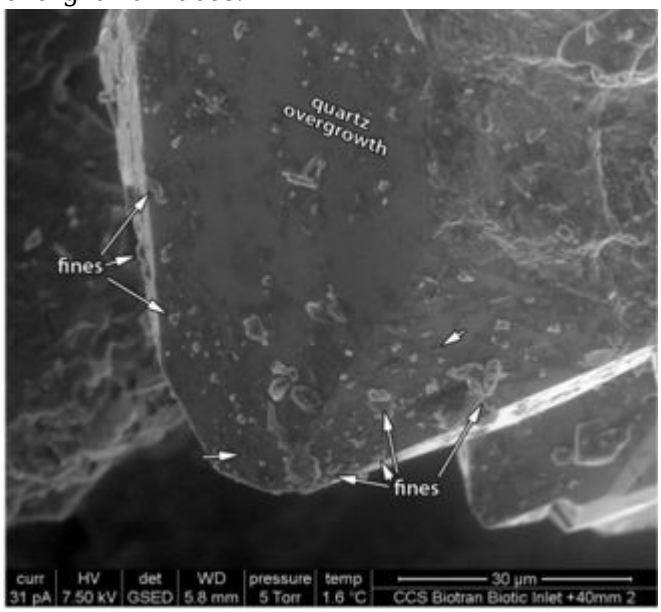

Plate 22 Post test biotic sample, edge inlet + 40 mm, 95% humidity. Patchy film and

associated fines on a protruding apical quartz overgrowth site. Film and fines are more abundant towards the tip. There are scattered rounded, oval <3 µm forms (unlabelled arrows).

Outlet

Film-like material similar to that observed in the rest of the sample is sparse, but identifiable at the outlet end both in central and edge (Plate 23) sites. No cell-like forms were recognised, however.

Examples of collapsed illitic fibres identified in the absence of film (Plate 24) show that the collapse is not necessarily related to the presence or formation of the film. Additionally, the presence of clusters of un-collapsed illitic fibres (Plate 25) shows that not all of this phase was collapsed state prior to testing, and that testing and analysis have not necessarily caused collapse.

- 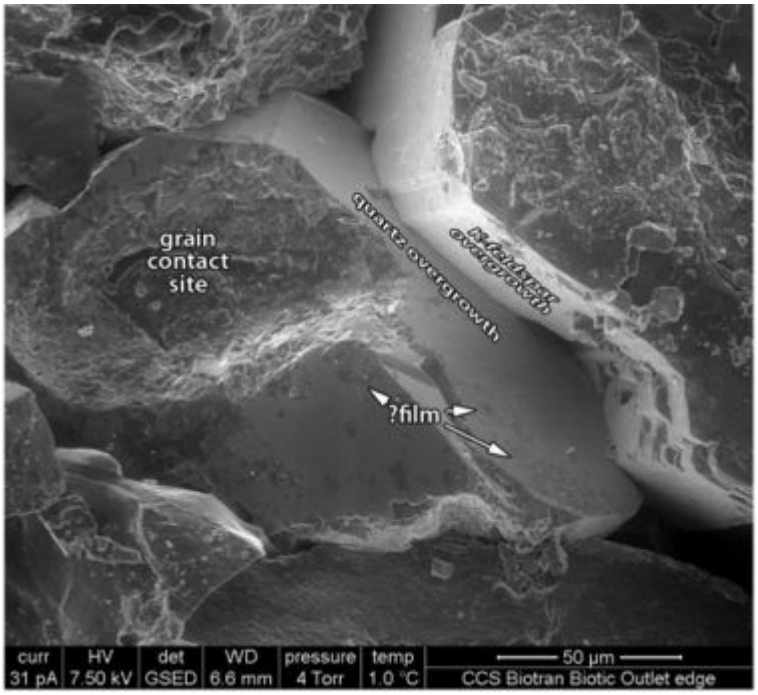

Plate 23 Post test biotic sample, edge outlet, 90% humidity. Pore-lining film is sparsely distributed at the outlet end of the sample both the edge sites (as shown here) and at central sites.

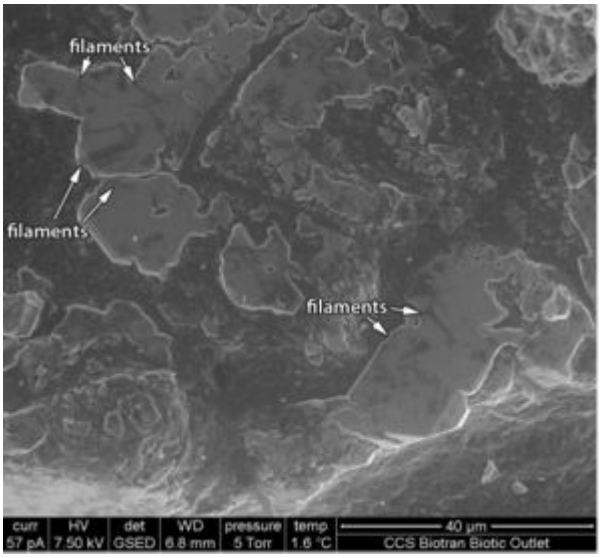

Plate 24 Post test biotic sample, central outlet, 90% humidity. Dark areas here are residual fluids on rougher pore walls and filamentous forms laid across a partially developed quartz overgrowth. These are illitic clay forms that are laid across the overgrowth surfaces; this probable collapse could have occurred prior to, during or after the testing.

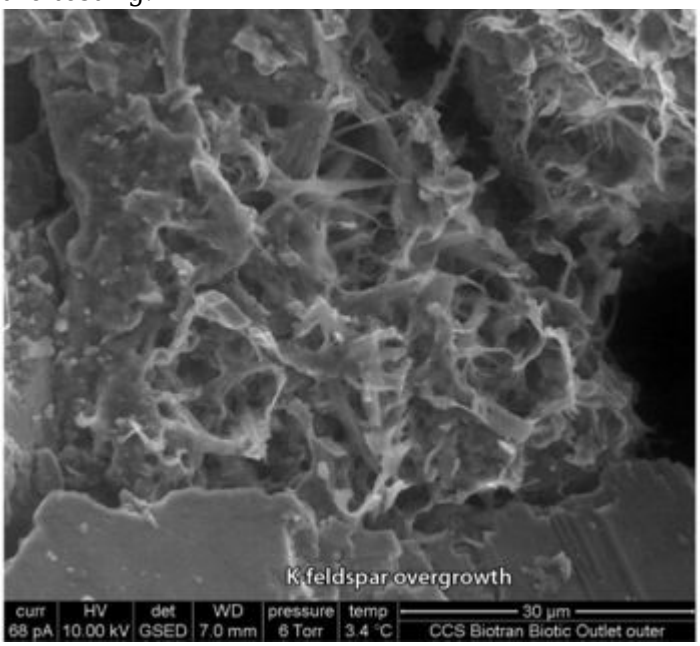

Plate 25 Post test biotic sample, edge outlet, 95% humidity. An example of a filamentous illitic clay cluster that has not collapsed. There is no evidence of film amongst the filaments.

Grey stained material

A sample prepared from the area of the outlet end of the post test plug with the grey stain was examined. Small patches of a surface coating with a droplet like morphology were noted (Plate 26). Droplets ranged from 10–20 µm in diameter. These droplets appear to be of a non-aqueous liquid phase, since they did not evaporate under reduced humidity conditions.

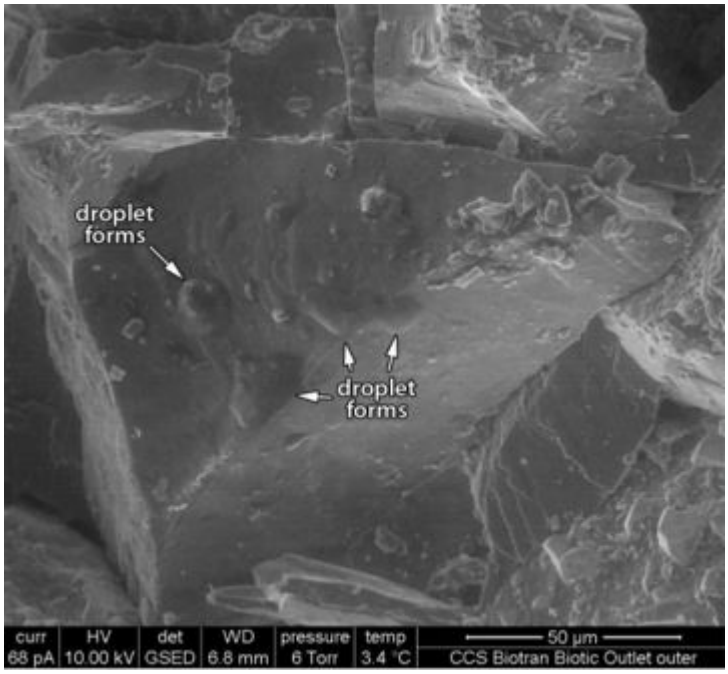

Plate 26 SEM image. Post test biotic sample, outlet end, grey stained area, 95% humidity. A sample portion prepared from the outer grey stained surface. There are localised areas with a coating of droplet-like forms. No other surface deposits were observed.

Microbiology

Mean total microbial counts, obtained by epifluorescence microscopy, for the fluids from the control (abiotic) and biotic experiment experiments are given in Tables 2 and 3 respectively.

Control column experiment

The control column experiment ran for 31 days (744 h) in total with no injection of live organisms, pressure changes were continuously monitored throughout the course of the test. Table 4 and Figure 4 show the microbial count observed in the control experiment and indicate that although no live organisms were added to the experiment, indigenous microbes were present. The mean microbial count over the duration of the experiment peaked at 426 h, however the number of microbes observed was not considered to be significantly different to those observed on previous or latter sampling days. The visual difference in microbial counts is shown in Plate 27. The residual fluid in the pump at the end of the experiment indicated a high microbial count. This is thought to be a result of contamination of the experimental procedure or indigenous microbes from the test core breeding in the nutrient rich fluid. Microbial migration from the core to the pump requires further investigation.

Table 4 Mean total microbial counts by epifluorescence microscopy of outflow fluids from the control experiment.

Sample Name	Sampling Date	Total Time (h)	Mean organisms ml^{-1}	Standard Error
Start up fluid	03/11/2011	0.00	0	0
CT1	08/11/2011	89.33	2.09×10^{6}	2.00×10^{5}
CT2	15/11/2011	257.33	2.40×10^{6}	1.12×10^{6}

CT3	22/11/2011	425.83	9.22×10^5	1.28×10^5
CT4	29/11/2011	594.49	2.64×10^4	2.83×10^4
*Fluid in pump	06/12/2011	761.33	2.41×10^6	1.00×10^6

Denotes microbial counts for fluid in the pump at the close of the experiment.

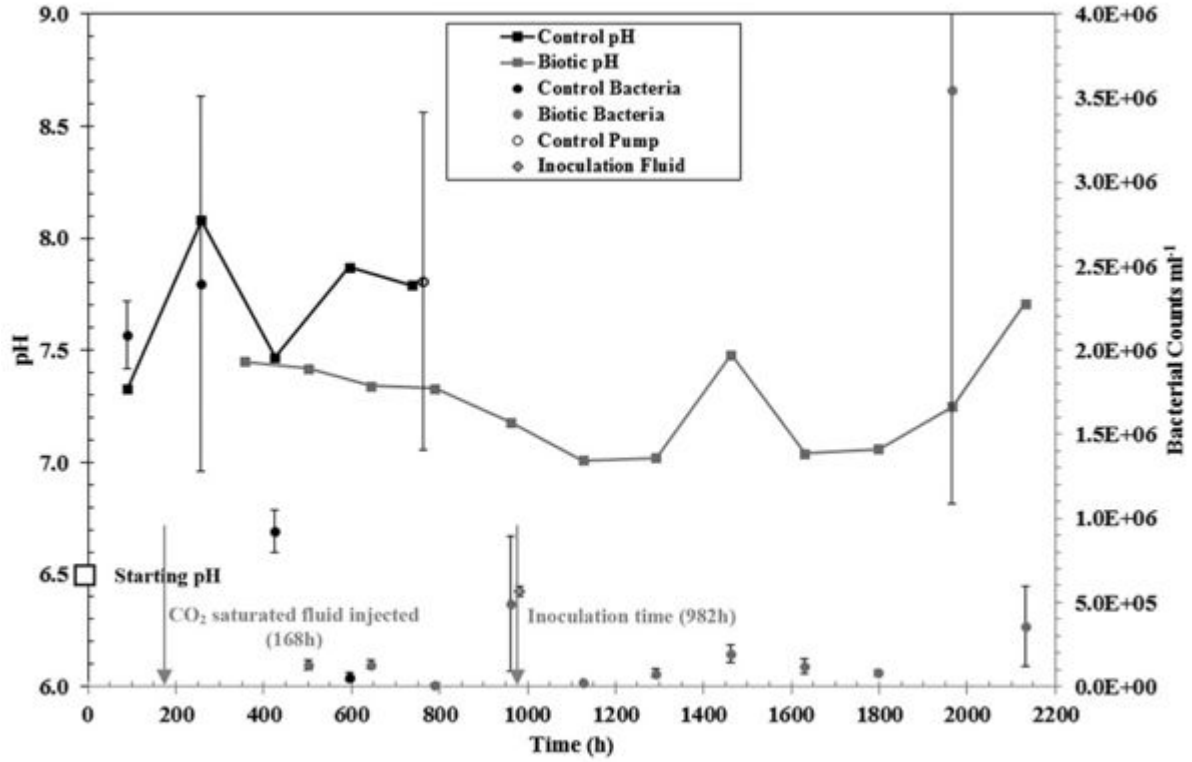

Figure 4 Microbial count and pH data for the control and biotic experiments. The control pH and microbial counts are shown by a black line a closed circles respectively with the biotic experiment represented by grey closed circles and line. The pH of the starting fluid in both experiments is shown by an open grey square. The number of microbes in the pump at the end of the control experiment are shown by an open black circle. The number of microbes in the inoculant for the biotic experiment are denoted by a closed grey diamond.

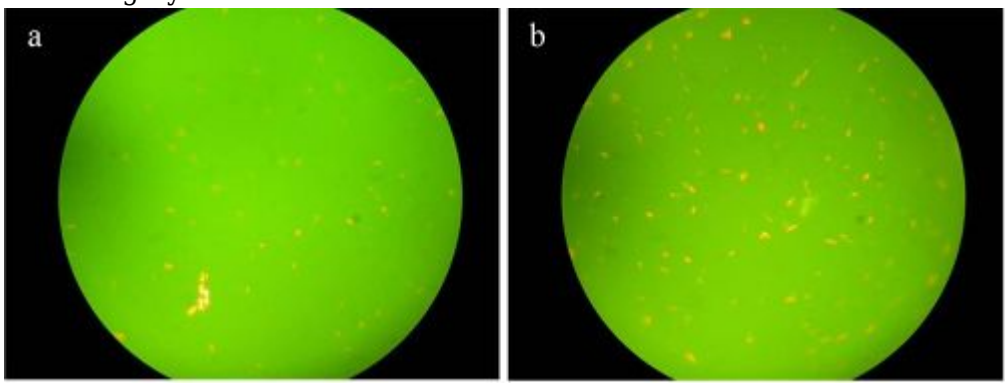

Plate 27 Epifluorescence photographs showing the microbes observed in control samples CT2 (a) and 3 (b).

Biotic column experiment

Sterile artificial groundwater was pumped through the core assembly for a nominal period (7 days – approx. 168 h) before the pump was stopped and CO_2 saturated groundwater injected. After a further 34 days, and a total of 41 days (981 h) after the start of the experiment, the pump was

stopped again and the *P. aeruginosa* bacteria injected.

Table 5 summarises the mean microbial counts collected from the outflow of the BFA at regular time intervals and the microbial count of the inoculant. Plate 28 shows epifluorescence images of samples CTCO-1, 9 and 11. Both Table 5 and Plate 28 indicate that the P. aeruginosa can survive in saline fluid saturated with CO_2. Examination of Plate 28 also shows differences in microbes with time. Plate 28a shows a relatively even spread of microbes at circa. 500 h, which has altered to a centralised mass of microbes, with other fluorescing material, that no longer covers the whole microscopic view at 1630 h (Plate 28b). At 1965 h into the biotic experiment, a loose mass of microbes were observed, central to the microscopic view, with few surrounding mircrobes (Plate 28c). Rod-like microbes were also observed, which were tentatively identified as bacillus.

Comparison of the number of viable microbes in the biotic experiment compared to the control experiment (Figure 4) indicates that the presence of CO_2 may restrict microbial activity. Subjective observation of the data presented in Plates 27b and 28a indicates that more microbes may be present in the biotic experiment thereby contradicting the microbial count data reported in Tables 4 and 5, which reports higher counts in the control experiments. This may be a function of the organisms clumping and therefore being more difficult to evaluate.

Table 5 Mean total microbial counts by epifluorescence microscopy of outflow fluids from the biotic experiment.

Sample Name	**Sampling Date**	**Total Time (h)**	**Mean organisms ml^{-1}**	**Standard Error**
CTCO2-1	23/12/2011	354.94	1.16×10^{7}	8.01×10^{5}
CTCO2-2	29/12/2011	500.61	1.28×10^{5}	2.66×10^{4}
CTCO2-3	04/01/2012	644.61	1.30×10^{5}	2.76×10^{4}
CTCO2-4	10/01/2012	788.28	1.13×10^{4}	6.06×10^{3}
CTCO2-5	17/01/2012	960.78	4.89×10^{5}	4.01×10^{5}
Inoculation fluid	18/01/2012	981.9	5.68×10^{5}	3.04×10^{4}
CTCO2-6	24/01/2012	1125.11	2.26×10^{4}	8.77×10^{3}
CTCO2-7	31/01/2012	1292.28	7.90×10^{4}	2.67×10^{4}
CTCO2-8	07/02/2012	1462.03	1.92×10^{5}	5.17×10^{4}
CTCO2-9	14/02/2012	1630.03	1.20×10^{5}	4.13×10^{4}
CTCO2-10	21/02/2012	1797.53	7.97×10^{4}	1.59×10^{4}
CTCO2-11	28/02/2012	1965.28	3.55×10^{6}	2.46×10^{6}
CTCO2-12	06/03/2012	2132.28	3.57×10^{5}	2.39×10^{5}

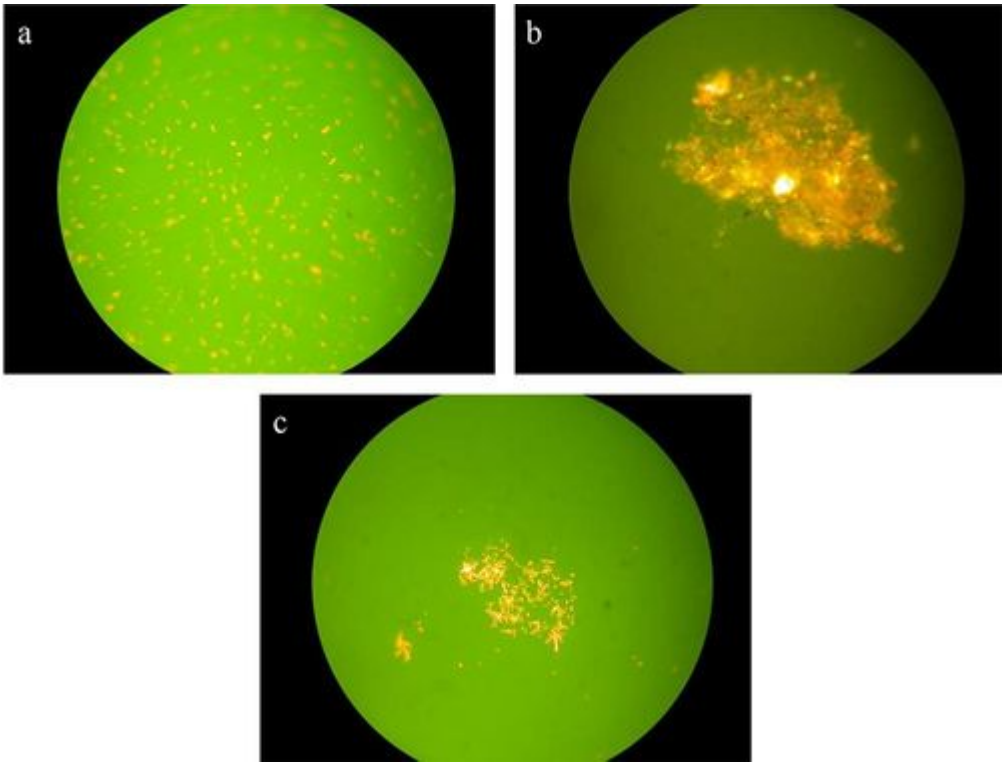

Plate 28 Epifluorescence photographs showing the microbes observed in biotic samples CTCO2-1 (a), CTCO2-9 (b) and CTCO2-11 (c).

Physical measurement results

Both control and biotic experiments were performed at a constant flow rate, changes in injection and confining pressure were continuously logged by pressure transducers. An overlay of the biotic and control pressure graphs from the start of the experiment to 2200 h is given in (Figure 16).

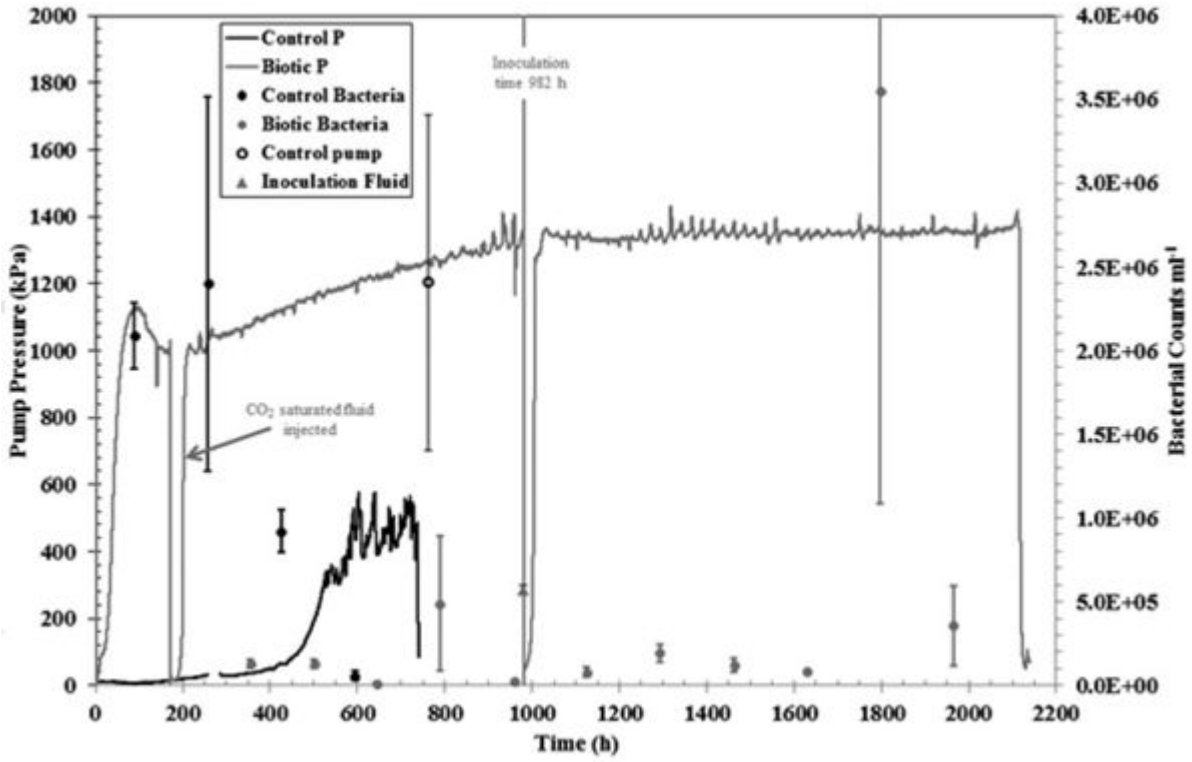

Figure 5 Overlay of recorded pressure and microbial counts in the outflow fluids from the control and biotic columns from the start of each experiment. Black lines and closed

circles relate to the control experiment and grey lines and closed circles the biotic experiment. The number of microbes in the inoculant, for the biotic experiment, is denoted by a closed grey triangle. The time of inclusion of saturated CO_2 fluid inoculation are marked on plot.

Figure 5 shows that for the control experiment the presence of backpressure was not evident until 400 h, at which point an increase was observed, reaching 400–600 kPa. This range of pressure was observed until termination of the control experiment and though to be associated with biological contamination of the sample, as although microbes were not injected into the system analysis of the outflow fluids indicates their presence after 100 h.

For the biotic core, Figure 5 shows an initial rapid increase in pressure up to circa. 1000 kPa, showing a distinct difference compared to the control core. This indicates a difference in the physical properties e.g. the heterogeneity of the two materials, although they were collected from side by side in the same original core material. The pressure in the biotic core steadily increases after the inclusion of CO_2 to the saline at 120 h to ca. 980 h, where the microbes were added. Beyond this point, the pressure, apart from minor variations, is effectively constant.

Fluid chemistry

The results of the fluid chemistry analysis for the control and biotic cores are tabulated in Appendices 2 and 3 respectively. Where data is reported as less than the limit of detection (LOD), the LOD is set at 0.5 multiplied by the analyte detection limit. Analyses for a number of analytes at the start of the control experiment appear to be spurious.

pH and alkalinity (HCO_3^-)

The pH measurements made on the control and biotic samples collected on removal from the BFA are summarised in Tables 6 and 7 respectively and represented graphically in Figure 4. Table 6 and Figure 4 show that the control pH ranged between 7.3 and 8.1 across the length of the experiment, with a mean pH of 7.7. The mean pH observed for the biotic column experiment was 7.3, lower than that observed for the control column, with a range of 7.0–8.1. Figure 4 indicates that for both the control and biotic columns, no correlation between pH and microbial counts was evident. The observed increase in pH up to ca. 700 h, in both experiments, compared to the starting fluid, indicates that the pH in both systems is buffered by the rock itself. After this period, in the biotic experiments, the fluid pH drops to ca. 7.0, which is higher than expected given the use of a CO_2 rich fluid. This also indicates that the rock itself is buffering any changes in pH. Figure 6 shows the changes in alkalinity, as HCO_3^-, in both the control and biotic experiments and the data is reported in Appendices 2 and 3. As the synthetic groundwater used in the experiment was a solution of NaCl supplemented with sodium acetate, the presence of HCO_3^- ions at a significant concentration would not be expected in the outflow fluids from the control column, which is evidenced by Figure 5. After saturation of the groundwater with CO_2, Figure 6 shows an increase of HCO_3^- ions at ca. 200 h to a relatively constant concentration of ca. 650 mg l^{-1} throughout the remainder of the experiment, indicating that the CO2 containing fluid remains stable with respect to CO_2 concentration.

Table 6 pH measurements for control samples.

Sample Name	Sampling Date	Total Time (h)	pH
CT1	08/11/2011 10:00	89.33	7.3
CT2	15/11/2011 10:00	257.33	8.1
CT3	22/11/2011 10:30	425.83	7.5

CT4	29/11/2011 11:00	594.33	7.9
CT5	05/12/2011 10:00	737.33	7.8

Table 7 pH measurements for biotic samples.

Sample Name	Sampling Date	Total Time (h)	pH
CTCO2-1	23/12/2011	354.94	7.5
CTCO2-2	29/12/2011	500.61	7.4
CTCO2-3	04/01/2012	644.61	7.3
CTCO2-4	10/01/2012	788.28	7.3
CTCO2-5	17/01/2012	960.78	7.2
CTCO2-6	24/01/2012	1125.11	7.0
CTCO2-7	31/01/2012	1292.28	7.0
CTCO2-8	07/02/2012	1462.03	7.5
CTCO2-9	14/02/2012	1630.03	7.0
CTCO2-10	21/02/2012	1797.53	7.1
CTCO2-11	28/02/2012	1965.28	7.3
CTCO2-12	06/03/2012	2132.28	7.7

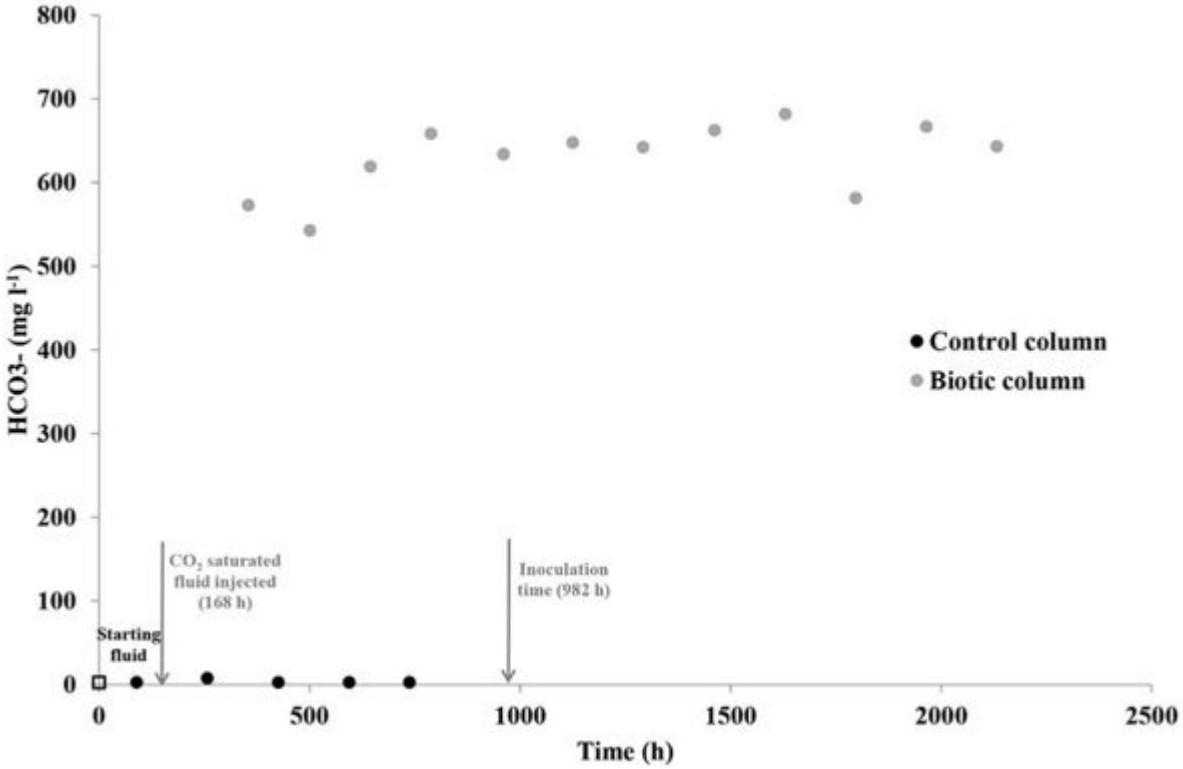

Figure 6 Alkalinity data measured as HCO_3^- for the control and biotic experiments. Closed black and grey circles represent the control and biotic experiments respectively. The HCO_3^- concentration in both starting fluids is shown by an open black square.

Sodium (Na) and Chloride (Cl)

Figures 7 and 8 show the Na and Cl concentrations in the output fluids from both the biotic and control experiments remain constant. This indicates that the major composition of the synthetic groundwater is not influenced by the presence of CO_2, the host rock core or the presence of micro-organisms.

Non Purgeable Organic Carbon (NPOC)

Figure 9 summarises the NPOC data for both columns and shows that the inoculation of organisms at 982 h results in an increase in the amount of soluble organic carbon.

Iron (Fe)

Figure 10 summarise the total Fe concentrations eluting from both columns. The data indicate that both the presence of CO_2 and microbes have little or no influence on the solubility of total Fe in this system. Reduced Fe (Appendix 2 and Appendix 3) is below the limit of detection.

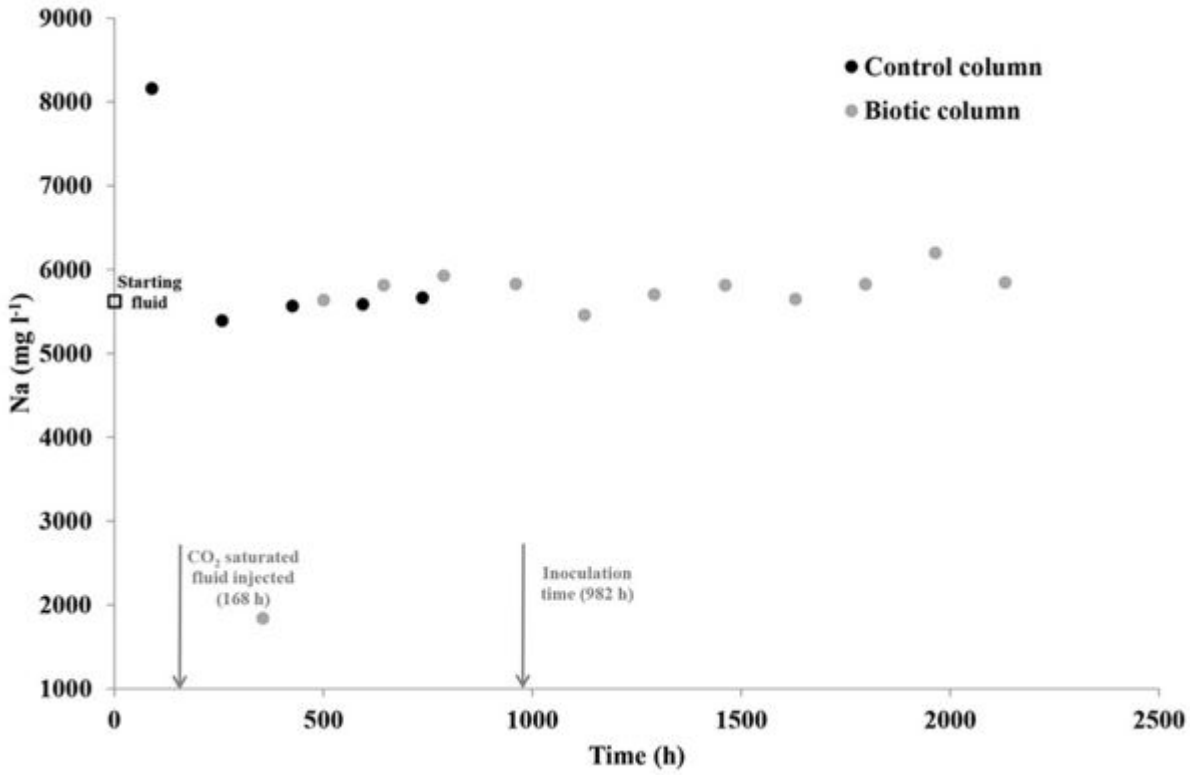

Figure 7 Sodium data for the control and biotic experiments. Closed black and grey circles represent the control and biotic experiments respectively. The sodium concentration in both starting fluids is shown by an open black square.

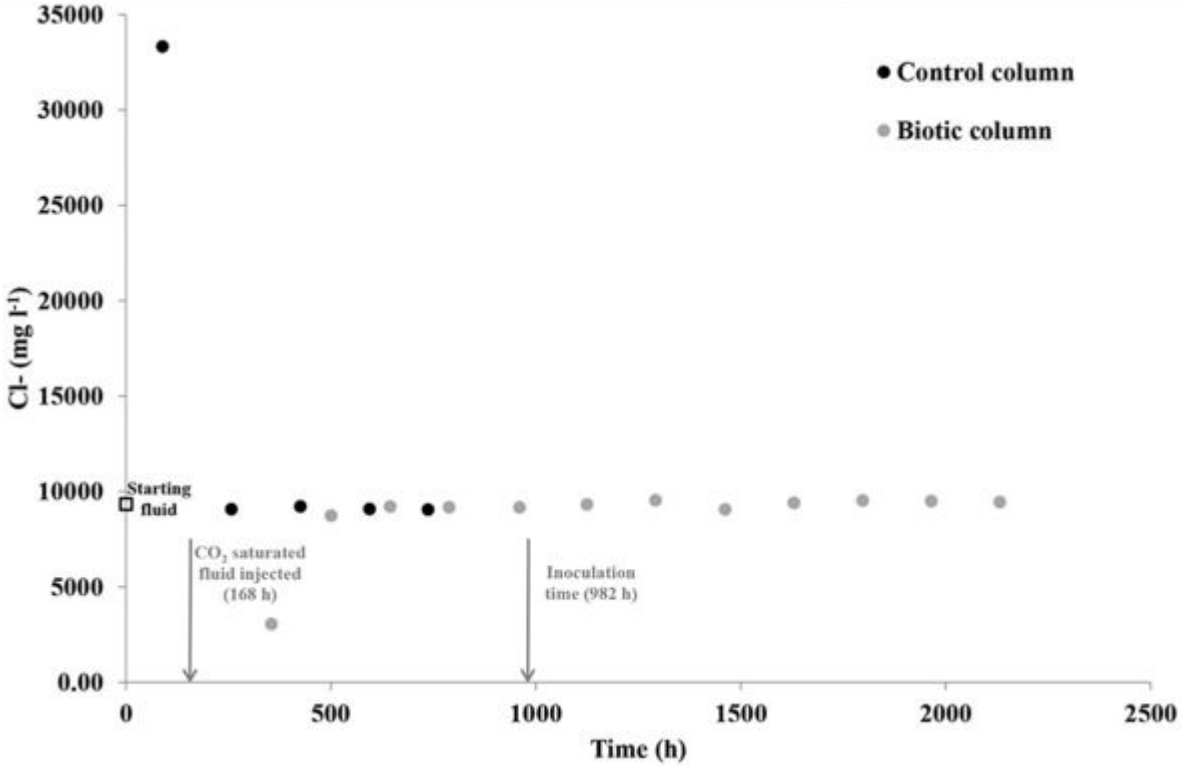

Figure 8 Chloride data for the control and biotic experiments. Closed black and grey circles represent the control and biotic experiments respectively. The chloride concentration in both starting fluids is shown by an open black square.

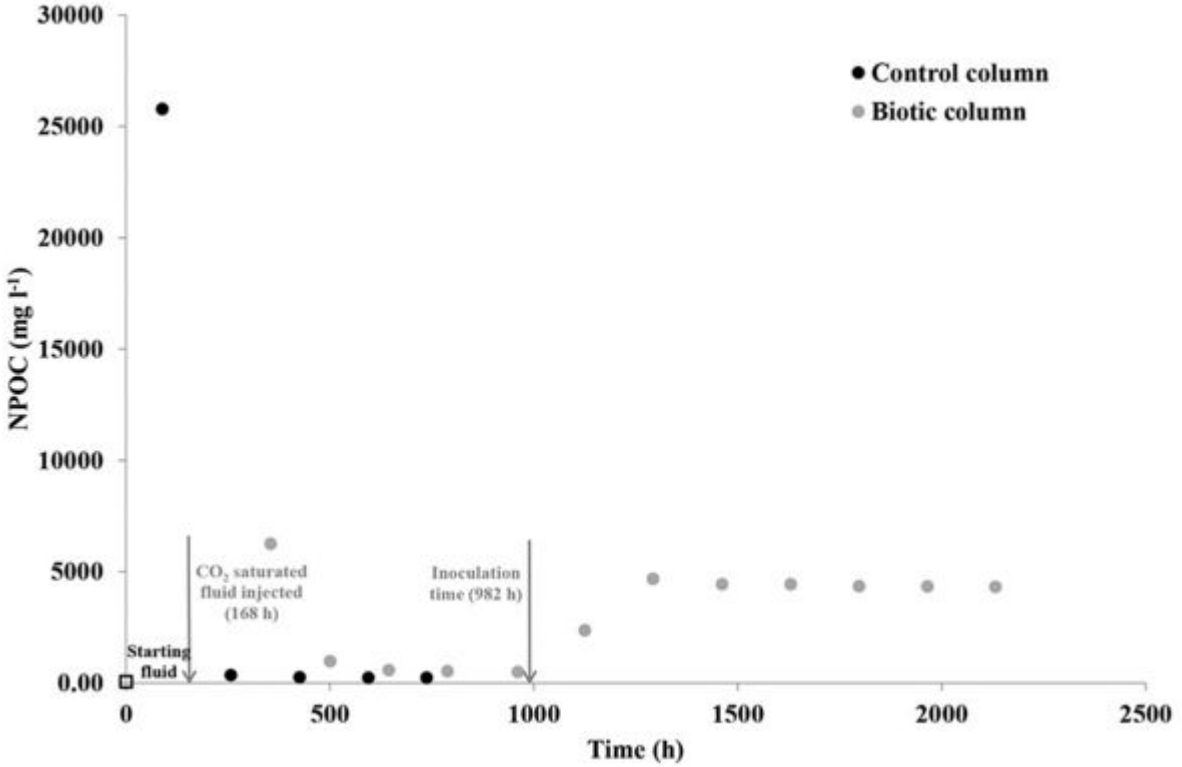

Figure 9 NPOC data for the control and biotic experiments. Closed black and grey circles represent the control and biotic experiments respectively. The NPOC concentration in both starting fluids is shown by an open black square.

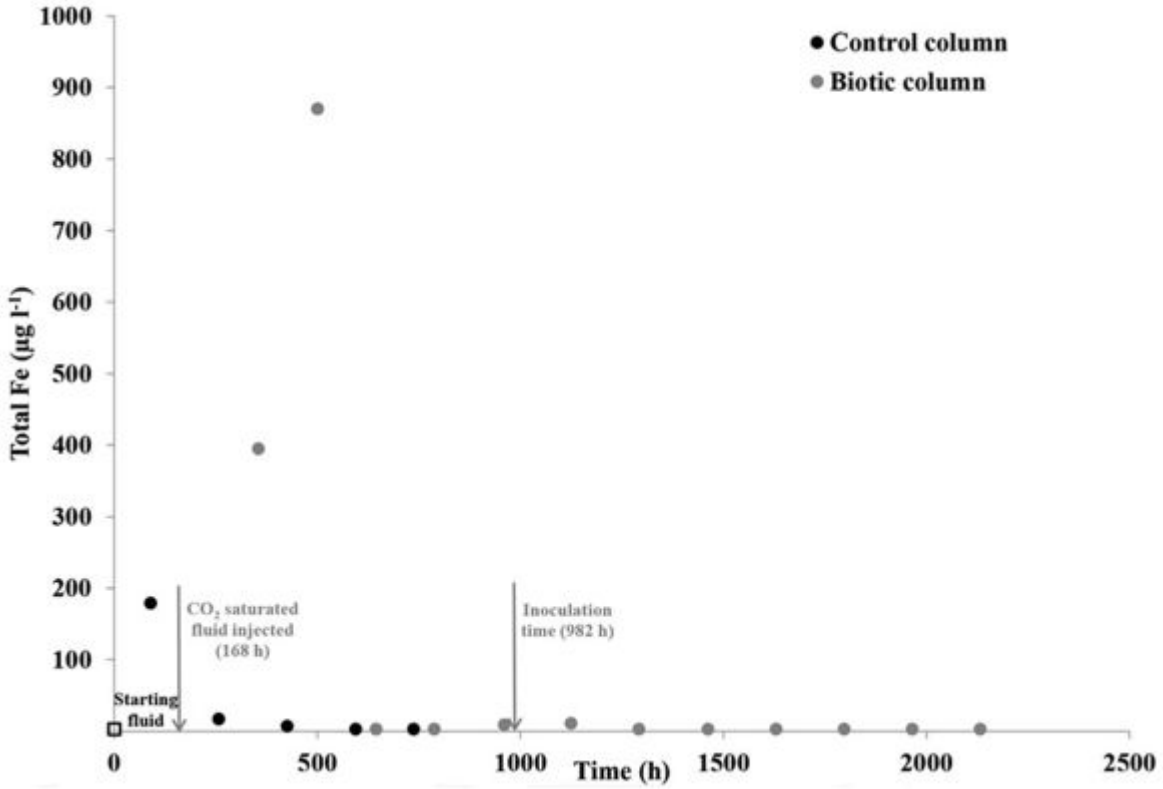

Figure 10 Total iron data for the control and biotic experiments. Closed black and grey circles represent the control and biotic experiments respectively. The iron concentration in both starting fluids is shown by an open black square.

Magnesium (Mg) and Nickel (Ni)

Figures 11 and 12 demonstrate that when CO_2 is introduced into the fluids the release of Mg and Ni is enhanced. The release of Ni may be a result of partial dissolution of the piping used in the BFA, as Ni is a component of steel; however this is unlikely because of the pH observed in the outflow fluids (Figure 4) is not acidic. The presence of Ni is more likely to be associated with the chlorite in the host rock material. The source of the Mg is most likely to be dolomite and/or chlorite, both Mg rich minerals identified as present in the post experiment host rock material (Table 2), which would dissolve in the presence of CO_2.

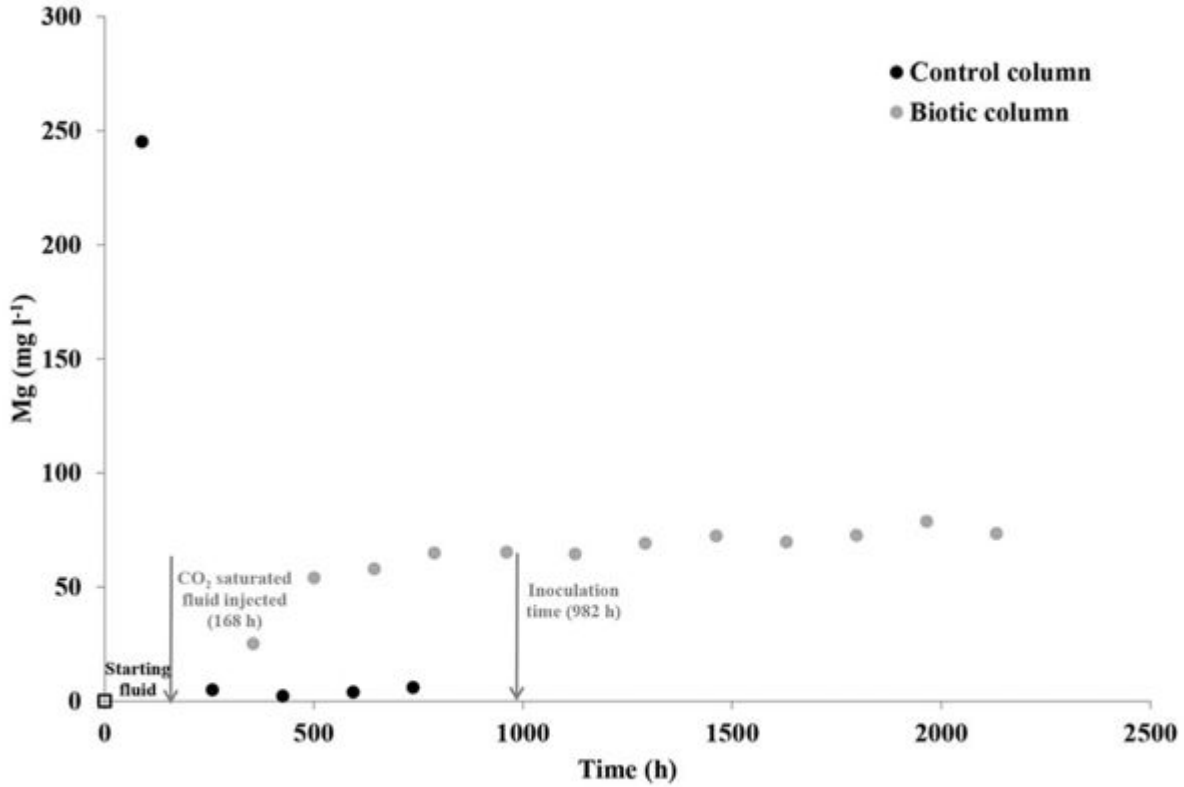

Figure 11 Magnesium data for the control and biotic experiments. Closed black and grey circles represent the control and biotic experiments respectively. The magnesium concentration in both starting fluids is shown by an open black square.

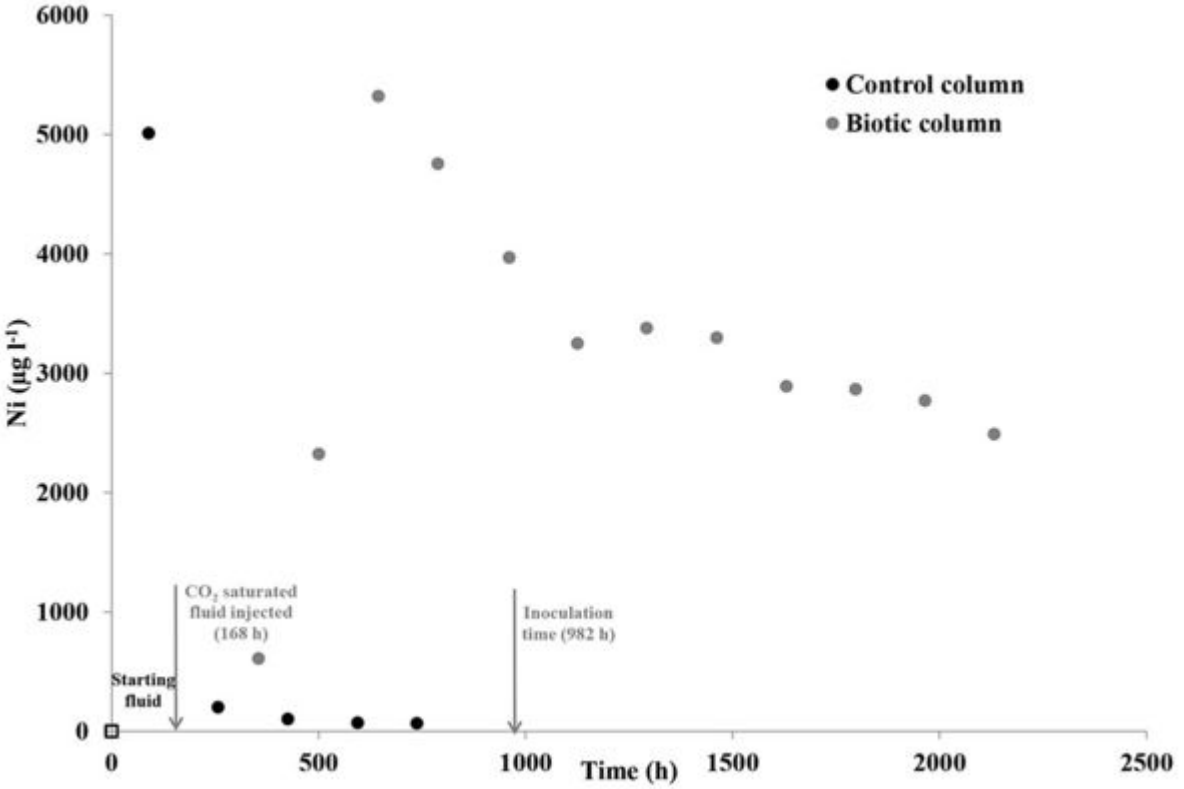

Figure 12 Nickel data for the control and biotic experiments. Closed black and grey circles represent the control and biotic experiments respectively. The nickel concentration in both starting fluids is shown by an open black square.

Potassium (K), Silicon (Si) and Antimony (Sb)

Figures 13–15 summarise the Si, K and Sb data for the two experiments. Figure 13 shows similar

trends for both experiments, where between ca. 250 and 600 h a peak is observed relating to the release of ca. 300–500 mg l^{-1} K. Chlorite, micas and k-feldspar are potential sources of the leachable K (Table 2). A similar trend is seen in Figure 15 for Sb, where ca. 2 ug l^{-1} is released over a slightly longer timescale (up to 1000 h). This is thought to be associated with the mobilisation of clay fines and the associated trace elements. It is also likely that Si associated with clay coatings is mobilised during both experiments (Figure 14). However, Figure 14 indicates that the release of Si is enhanced in the biotic experiment when compared to the control.

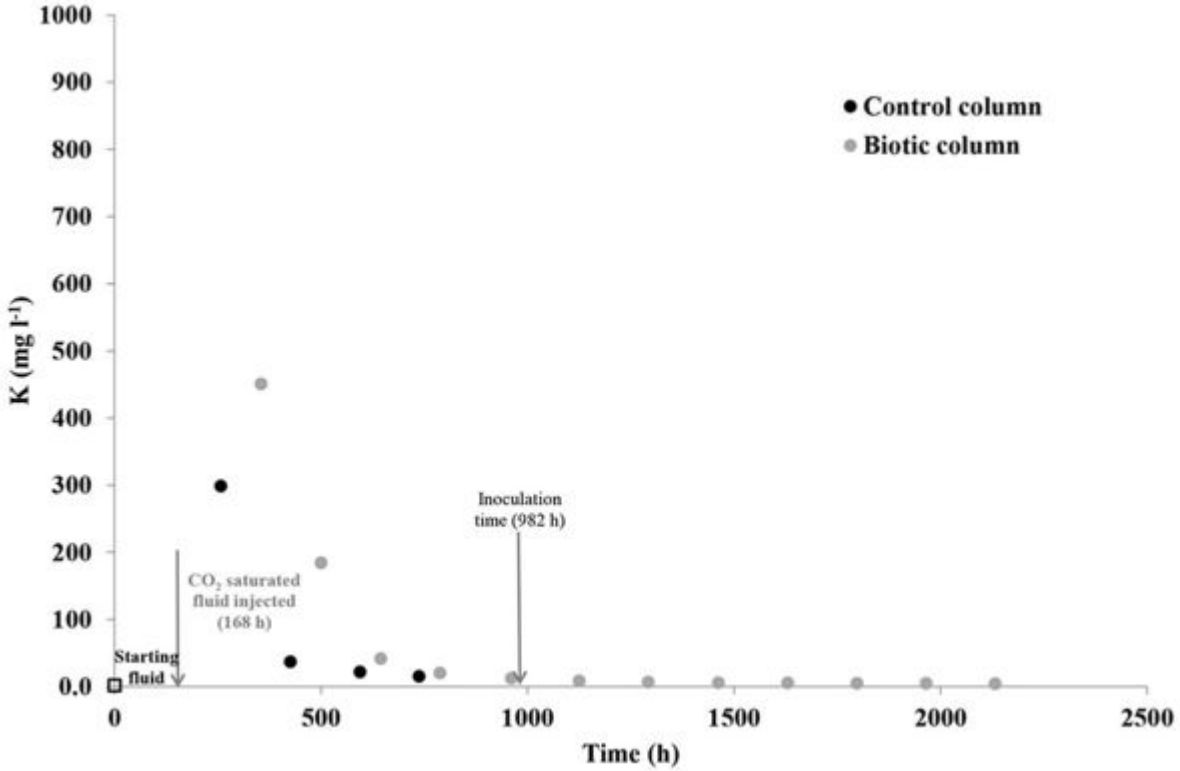

Figure 13 Potassium data for the control and biotic experiments. Closed black and grey circles represent the control and biotic experiments respectively. The potassium concentration in both starting fluids is shown by an open black square.

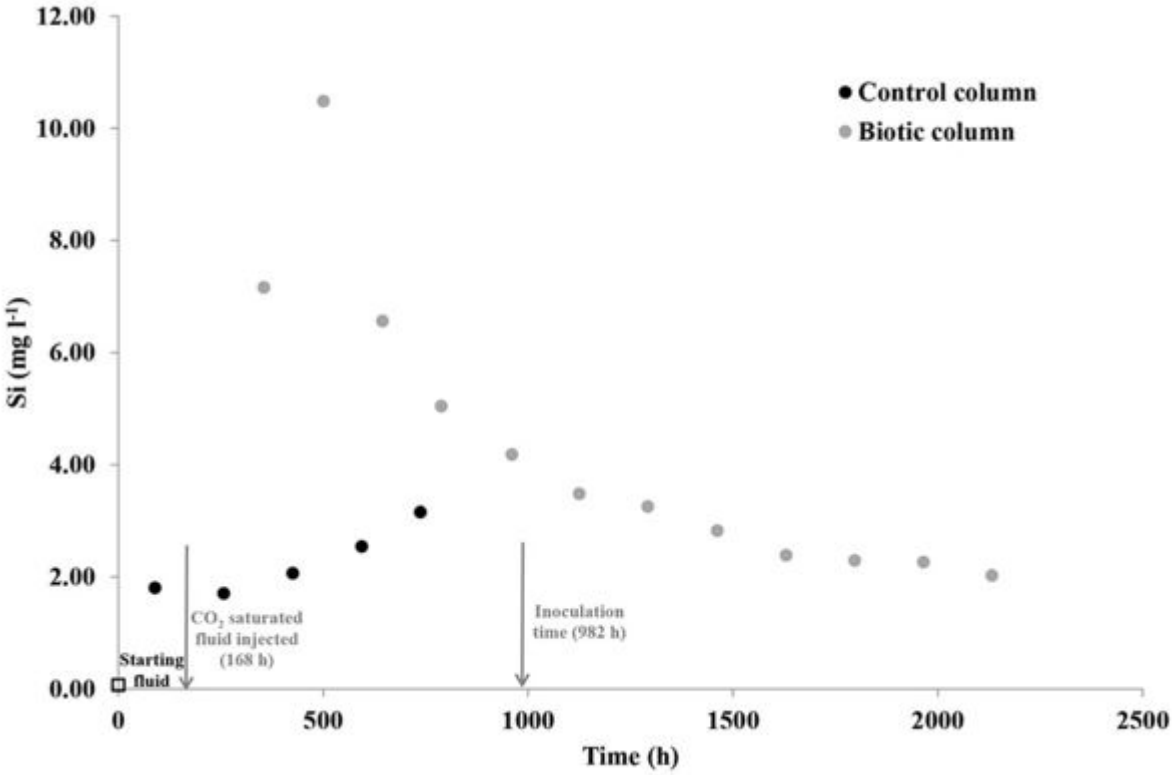

Figure 14 Silicon data for the control and biotic experiments. Closed black and grey circles represent the control and biotic experiments respectively. The silicon concentration in both starting fluids is shown by an open black square.

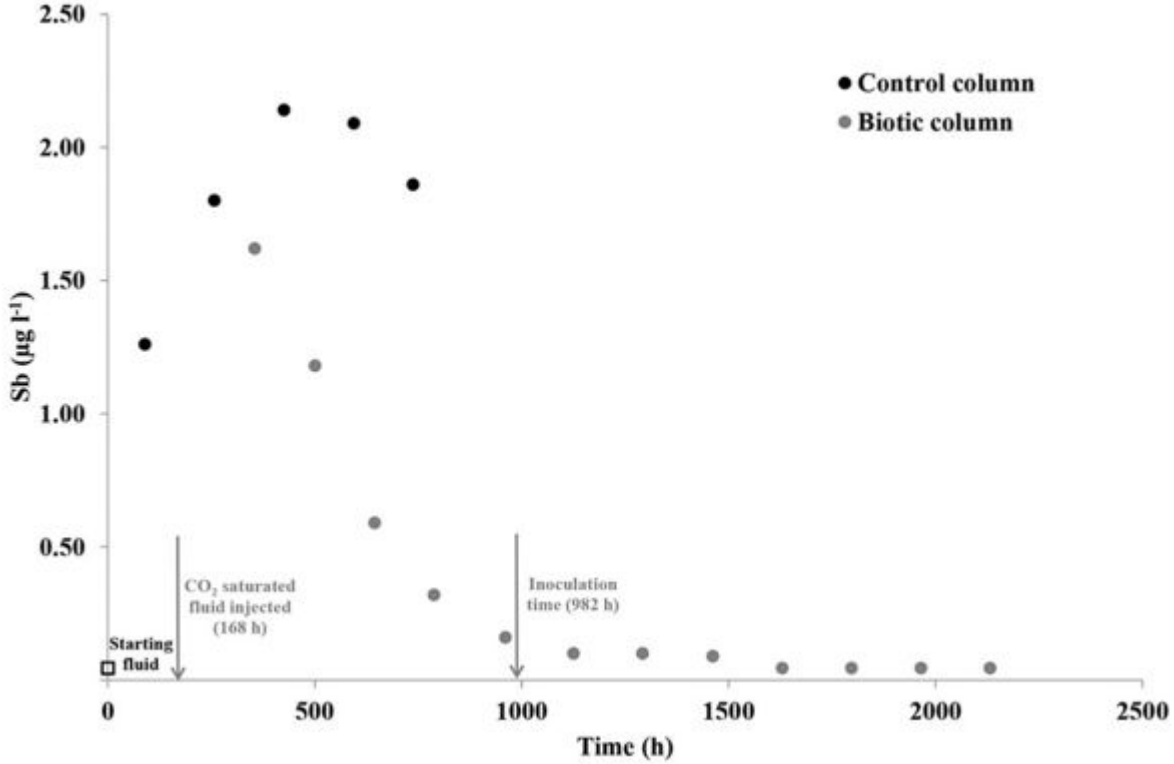

Figure 15 Antimony data for the control and biotic experiments. Closed black and grey circles represent the control and biotic experiments respectively. The antimony concentration in both starting fluids is shown by an open black square.

Tungsten

Figure 16 shows the release of W in both experiments over time. Peaks early (ca. 300 h) in both the control and biotic experiments suggest the presence of relatively mobile W. A possible source of W is

the W-carbide cutting blade, used to prepare the core materials.

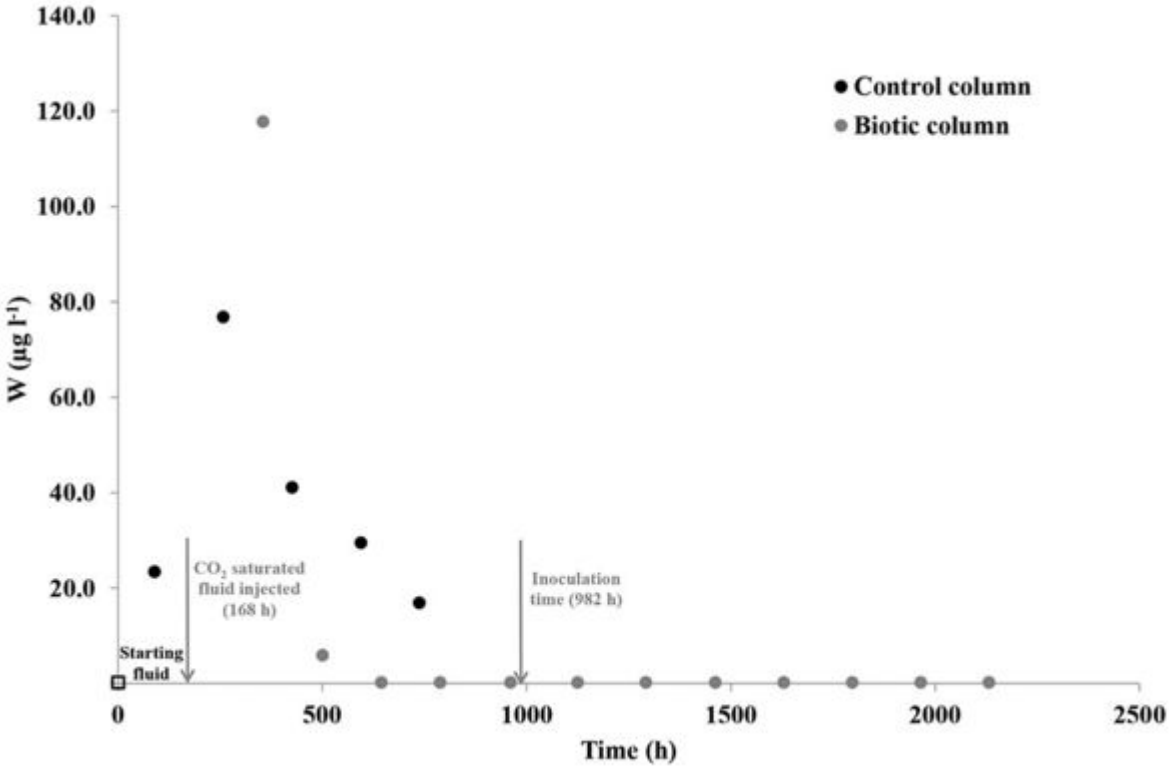

Figure 16 Tungsten data for the control and biotic experiments. Closed black and grey circles represent the control and biotic experiments respectively. The tungsten concentration in both starting fluids is shown by an open black square.

References

1. ↑ WEST, J M, MCKINLEY, I G, PALUMBO-ROE, B, and ROCHELLE, C A. 2011. Potential impact of CO2 storage on subsurface microbial ecosystems and implication for groundwater quality. Energy Procedia, 4, 3163–3170. doi:10.1016/j.egypro.2011.02.231.

Retrieved from 'http://earthwise.bgs.ac.uk/index.php?title=OR/12/023_Results&oldid=44862'
Category:

- OR/12/023 Microbial Impacts of CO2 transport in Sherwood Sandstone

Navigation menu

Personal tools

- Not logged in
- Talk
- Contributions
- Log in
- Request account

Namespaces

- Page
- Discussion

☐

Variants

Views

- Read
- Edit
- View history
- PDF Export

☐

More

Search

Search Go

Navigation

- Main page
- Recent changes
- Random page
- Help about MediaWiki

Tools

- What links here
- Related changes
- Special pages
- Permanent link
- Page information
- Cite this page
- Browse properties

- This page was last modified on 18 December 2019, at 12:12.

- Privacy policy
- About Earthwise
- Disclaimers
-

-